Arabian Journal of Geosciences (2021) 14: 1626
https://doi.org/10.1007/s12517-021-08140-w

ORIGINAL PAPER

Dynamics of a subvolcanic magma chamber inferred from viscous instabilities owing to mafic-felsic magma interactions

Bibhuti Gogoi[1] · Hiredya Chauhan[2]

Received: 17 February 2021 / Accepted: 27 July 2021 / Published online: 2 August 2021

Abstract

The Ghansura Rhyolite Dome (GRD) of Chotanagpur Granite Gneiss Complex, eastern India, presents an ideal geological setting to understand the dynamics of a subvolcanic magma chamber. The GRD was a shallow-level felsic magma chamber that was intruded by mafic/basaltic magma during its evolution leading to the formation of a variety of magma mixing and mingling zones. The first zone is composed of mafic rocks with felsic clasts. The second zone depicts mingled rocks where amphibole-rich microzones (ARM) and viscous folding are observed. The third zone represents non-porphyritic intermediate rock displaying emulsion texture. The fourth zone is composed of porphyritic intermediate rock displaying synneusis. From field relations, textural features, and mineral chemical data interpretations, it is inferred that the GRD was a zoned magma chamber when crystal-rich mafic magma intruded it. The felsic reservoir consisted of four distinct zones at the time of intrusion of the mafic magma. The outermost zone was completely solid, while the innermost zone was entirely melt. Between these two zones, there were two transitional physical boundary layers—the High-Viscosity Outer Transitional Zone (HVOTZ) that was in contact with the solid zone and the Low-Viscosity Inner Transitional Zone (LVITZ) that was in contact with the melt. Each individual layer interacted with the mafic magma differently to form discrete hybrid rocks. The outermost solid zone produced mafic rocks with felsic clasts, while the innermost melt zone produced porphyritic intermediate rock displaying synneusis. The HVOTZ interacted with the mafic magma to form mingled rocks where ARM and viscous folding are preserved. Lastly, the LVITZ interacted with the invading mafic magma to form non-porphyritic intermediate rock displaying emulsion texture.

Keywords Magma mixing and mingling · Subvolcanic magma chamber · Felsic clasts · Viscous folding · Emulsion texture · Synneusis

Introduction

Magma chambers are one of the most enigmatic features of our planet. Particularly important are the shallow-level crustal magma chambers that feed a large number of volcanic eruptions worldwide. Limited insight is available about the dynamics of such shallow reservoirs. This is because information about these enigmatic bodies is mostly acquired from expelled volcanic products (Wolff et al. 1999; Wolff and Ramos 2003; Bachmann and Bergantz 2004; Singer et al. 2014) or by using seismic tomography or other geophysical methods (Romero et al. 1993; Steck et al. 1998; Lowenstern et al. 2006; Tizzani et al. 2009; Farrell et al. 2014). Many studies have now revealed that magma chambers may be internally zoned having discrete rheological boundaries (Hildreth and Wilson 2007; Takahashi and Nakagawa 2012; Singer et al. 2014).These rheological boundaries occur within a magma chamber due to the variation in crystallinity in the magma (Gogoi et al. 2018a). The zoned structure in a single magma body is argued to have formed by fractional crystallization (McBirney 1980; Spera et al. 1984). The internal structure of such zoned magma chambers can be predicted from temporal changes in the eruptive materials of a single eruption sequence (Takahashi and Nakagawa 2012). However, analysis of such eruptive products spewed during volcanic eruptions serves as an indirect method to know about the processes

Responsible Editor: Domenico M. Doronzo

✉ Bibhuti Gogoi
bibhuti.gogoi.baruah@gmail.com

[1] Department of Geology, Cotton University, Guwahati, Assam 781001, India

[2] EPMA Laboratory, Department of Geology, Centre of Advanced Study, Banaras Hindu University, Varanasi 221005, India

operating in a magma chamber, and hence, this procedure may fail to provide us complete information about magma chamber dynamics.

An important phenomenon that frequently occurs in crustal magma reservoirs is the intrusion of compositionally different magmas. Such intrusions may lead to the mixing of disparate magmas and formation of hybrid rocks (DePaolo 1981; Grove et al. 1988; Hawkesworth et al. 2000). In fact, magma mixing happens to be a primary mechanism causing volcanic eruptions. When a compositionally distinct magma is injected into an already existing magma reservoir, the consequent influx of volatiles and the thermal disequilibrium generated may trigger eruptions (Sparks et al. 1977; Huppert et al. 1982; Sosa-Ceballos et al. 2012). Although magma mixing is a well-established phenomenon, we are still far away from understanding even the basic physico-chemical mechanisms associated with magma interactions and their potential impact upon our understanding of magmatic systems (Perugini and Poli 2012; Sosa-Ceballos et al. 2012; Farner et al. 2014). It is now widely accepted that mixing between two disparate magmas occurs through the combination of mechanical and chemical processes. Mixing is facilitated when any particle of one magma is brought closer to particles of the other (Snyder 1997). Hence, the two magmas must be mechanically stretched and folded leading to the development of chaotic mixing dynamics (Ottino 1989; Aref and El Naschie 1995). The onset of chaotic mixing produces filaments at several length scales, which is a prerequisite for efficient mixing (Perugini et al. 2002; DeCampos et al. 2011). While all of this occurs, the contact area between the two magmas increases exponentially, resulting in enhanced chemical exchanges through chemical diffusion. When the thickness of the filaments of both magmas becomes significantly small, diffusion homogenizes the two fluids into one, such that a homogenous mixture is produced. Such homogeneous mixtures form mixed rocks. On the other hand, incomplete diffusion leads to the preservation of filaments formed by stretching and folding of the two magmas, giving rise to heterogeneous mixtures that form mingled rocks.

There is a common consensus that textural features preserved in hybrid rocks can play a vital role in deciphering the behavior of two disparate magmas during their mixing (Hibbard 1981; Vegas et al. 2011; Charreteur and Tegner 2013; Gogoi et al. 2017). Textural constraints can also play an important role in understanding magma chamber dynamics (Agangi et al. 2011; Renjith et al. 2014; Weidendorfer et al. 2014). This study focuses on understanding the lesser known facts about the dynamics of magma mixing, and how mixing between two compositionally distinct magmas could dictate the mechanical evolution of a magma reservoir. Here we are trying to understand the dynamics of a shallow-level felsic magma chamber, presently exposed as the Ghansura Rhyolite Dome (GRD) in the Bathani volcano-sedimentary sequence (BVSs). The GRD preserves a variety of hybrid rocks, which resulted from the mixing and mingling of an invading crystal-rich mafic magma with the felsic host. The textural features preserved in the hybrid rocks of our study domain, which include felsic clasts, viscous folding, emulsions, and synneusis, provide significant clues to understand the nature of mixing that occurred between the mafic and felsic magmas. For this, we have integrated textural and mineral chemical data interpretations with some of the results obtained from microfluidic experiments, as microfluidics can significantly contribute toward understanding the dynamics of magma mixed systems. The primary objective of this work is to elucidate the role of two types of viscous instabilities (i.e., viscous folding and viscous swirling) produced during mafic-felsic magma interactions in deciphering the physical conditions of the felsic magma chamber. The experiments related to viscous folding and viscous swirling are carried out in microfluidic devices where viscous fluids like isopropanol alcohol, silicone oils (polydimethylsiloxane oils), and aqueous glycerol solutions are generally used (Cubaud and Mason 2007, 2008; Chung et al. 2010; Darvishi and Cubaud 2012). In these experiments, threads and jets of high viscosity fluids are focused in plane microchannels containing low viscosity fluids. As the viscous threads propagate through the less viscous fluids, the former may undergo an array of viscous instabilities due to the action of viscous and capillary forces. These instabilities increase the interfacial area between the two fluids, which leads to enhanced diffusion and mixing (Richards et al. 1994; Cubaud and Mason, 2006a, b).

Geological setting

The Ghansura dome is an integral part of the BVSs. The BVSs has been designated as the eastern extension of the Mahakoshal Mobile Belt of Central India Tectonic Zone (CITZ) (Saikia et al. 2014, 2017, 2019). The CITZ is an approximately 1,500 km long Proterozoic mobile belt running through the heart of peninsular India (Fig. 1). The ENE-WSW trending orogenic mobile belt marks the suturing of the North Indian Block (NIB) and the South Indian Block (SIB) to form the Greater Indian Landmass during the Proterozoic (Gogoi et al. 2020a). The NIB is composed of the Archean Bundelkhand Craton, whereas the SIB is a composite assemblage of the Dharwar, the Bastar, and the Singhbhum Archean cratons. The Proterozoic mobile belt consists of three broad domains from west to east, namely, the main CITZ occupying the central region of mainland India, the Chotanagpur Granite Gneiss Complex (CGGC) lying east of the main CITZ, and the easternmost Shillong Plateau Gneissic Complex. The BVSs is located at the northern fringe of the CGGC and constitutes an important magmatic assemblage of the broad tectonic domain (Fig. 1).

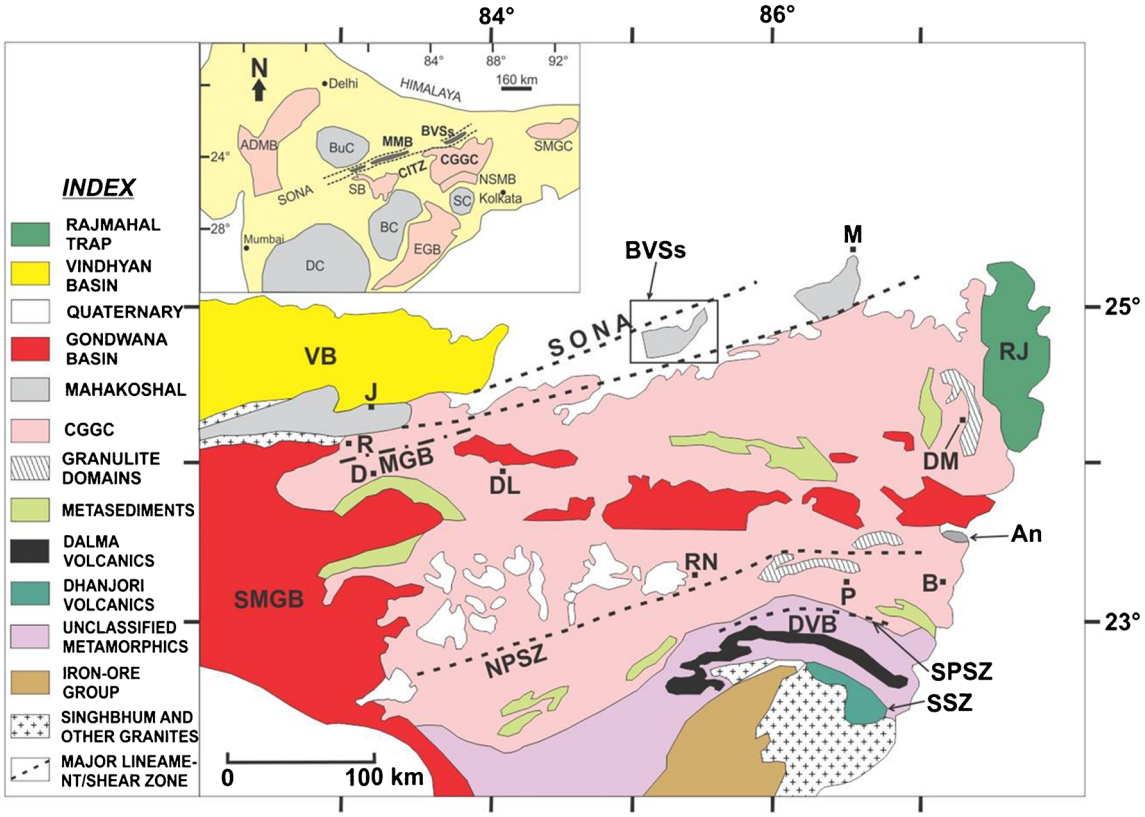

Fig. 1 Geological map of the Chotanagpur Granite Gneiss Complex (CGGC) (modified after Acharyya 2003). Abbreviations: An anorthosite, B Bankura, BVSs Bathani Volcanic and volcano-sedimentary sequence, D Dudhi, DL Daltonganj, DM Dumka, DVB Dalma Volcanic Belt, J Jirgadandi, M Munger, MGB Makrohar Granulite Belt, NPSZ North Purulia Shear Zone, PR Purulia, R Rihand–Renusagar Area, RJ Rajmahal Hills, RN Ranchi, SMGB Son Mahanadi Gondwana Basins, SPSZ South Purulia Shear Zone, SSZ Singhbhum Shear Zone, SONA Son Narmada Lineament, VB Vindhyan Basin. Inset shows the location of CGGC in the tectonic framework of the Archean cratonic blocks and Proterozoic mobile belts of India including Central India Tectonic Zone (CITZ), Eastern Ghats Belt (EGB), Aravalli Delhi Mobile Belt (ADMB), Shillong Meghalaya Gneissic Complex (SMGC), and North Singhbhum Mobile Belt (NSMB). Four Archean cratonic nuclei of India, namely Bastar Craton (BC), Singhbhum (SC), Bundelkhand (BuC), and Dharwar (DC), are shown (modified after Chatterjee and Ghose 2011)

The BVSs is a bimodal volcanic and volcano-sedimentary suite exposed at the northern margin of the CGGC (Ahmad and Wanjari 2009; Ahmad and Dubey 2011; Ahmad and Paul 2013; Ahmad et al. 2021). The sequence extends over a known aerial distance of approximately 40 km, with the type area located at Bathani village (24° 59.5′ N, 85° 16′ E) of Nalanda district, Bihar, India (Fig. 2a). The volcano-sedimentary unit comprises garnet-mica schist, rhyolite, tuff, banded iron formation, chert bands, and carbonate rocks, whereas the differentiated volcanic sequence comprises rhyolite, andesite, pillow basalt, massive basalt, tuff, and mafic pyroclasts. Granites were emplaced later that occur as small hillocks and plutons crosscutting the volcanic sequence. The granitic magmatism of the BVSs has been related to the Columbia supercontinent assembly (2000–1700 Ma) (Saikia et al. 2017; Saikia et al. 2019). On the basis of primary sedimentary and volcanic structures, it may be established that the volcano-sedimentary sequence is overlain by the differentiated volcanic sequence, and there is no remarkable break between the two sequences. The association of pillow lava, rhyolite, explosive fragments, and volcanogenic and chemogenic sediments suggests eruption of mafic/felsic magmas and ejection of pyroclasts in subaqueous condition. Subaqueous emplacement of mafic lavas associated with pyroclasts is a characteristic feature of subduction zones associated with island arc or even ophiolites belts around the world (Wilson 1989).

Field relationships

The Ghansura dome is a small felsic domain occurring in the BVSs at Ghansura village near Bathani, which at the outcrop scale preserves good evidence of magma mixing and mingling (Fig. 2b; Gogoi et al. 2018b). From field observations, it appears that the GRD shares crosscutting relationship with the volcano-sedimentary unit suggesting that the dome was emplaced at a later stage in the BVSs (Fig. 2a). A wide variety of rock types are encountered in the felsic dome ranging from mafic to felsic. Other than the mafic and felsic rocks, four

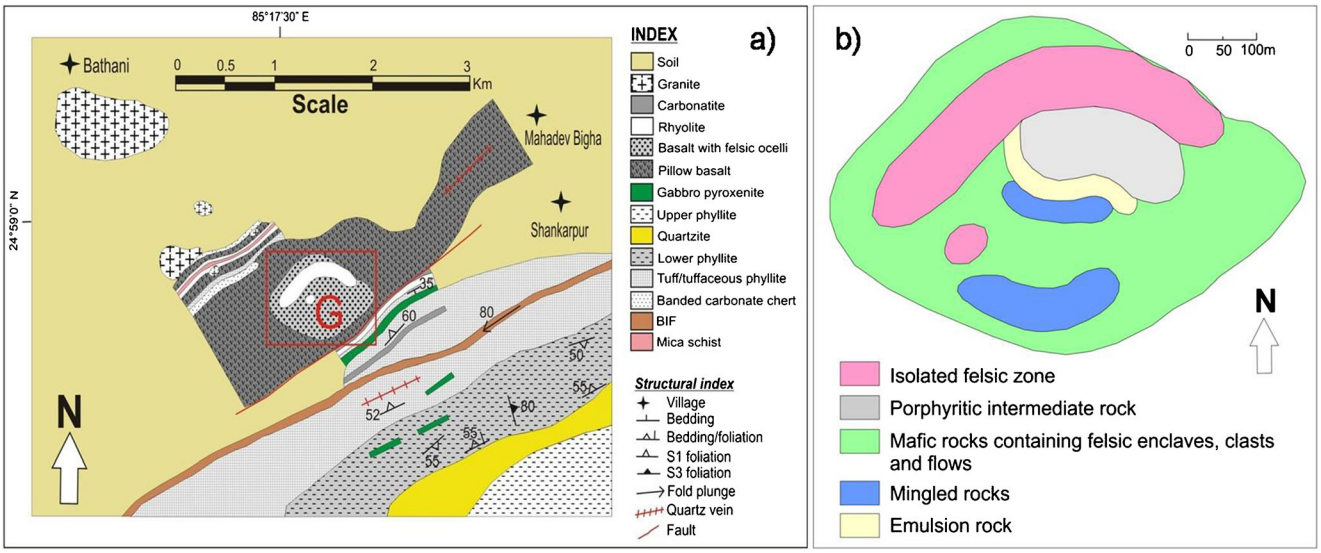

Fig. 2 **a** Geological map of the Bathani volcano-sedimentary sequence showing the locations of various litho-units. The Ghansura Rhyolite Dome is marked on the map as "G" (modified after Ahmad and Paul 2013). **b** Simplified geological map of the Ghansura Rhyolite Dome showing the disposal of various litho-units

distinct hybridized rocks are encountered. The hybrid rocks include mafic rocks containing felsic clasts, mingled rocks, porphyritic rock, and emulsion rock. These rocks appear to have formed from different degrees of interaction between the mafic and felsic magmas. The mafic rocks with felsic clasts are characterized by fine-grained leucocratic fragments of variable size embedded in melanocratic mafic groundmass. The mingled rocks are characterized by coexistence of mafic and felsic rocks produced due to intermingling of the two magmas. The porphyritic rock is a gray-colored homogeneous mixed rock in which individual components of the mafic and felsic magmas could not be identified. The emulsion rock is characterized by a fine comingled texture in which darker mafic emulsions occur within a gray-colored groundmass. A brief description of each of the hybrid rocks is given below:

a) The first category of hybrid rock is represented by mafic rocks containing angular clasts of the felsic host (Fig. 3a). At a few locations, sharp contact between this hybrid rock and the host rhyolite is clearly visible (Fig. 3b). There are certain zones in which the mafic rocks contain abundant felsic clasts with reaction surfaces (Fig. 3c). The felsic rock components of various shapes and sizes are embedded within fine-grained mafic groundmass. The felsic fragments greatly vary in size ranging from 1mm to about 5 cm. Most of them appear to be ellipsoidal in shape. Occasionally, felsic clasts are stretched out to thin streaks. The clasts are relatively finer with respect to the mafic rocks. The host mafic groundmass is highly vesicular. The felsic clasts display all degrees of coalescing and juxtaposition. They may be juxtaposed, they may merge, or multiple clasts may coalesce into larger domains of up to 20 cm in size. The clasts neither show any radial internal structure, nor do they display zoning. Their color ranges from white to light gray. Contacts between the felsic rock fragments and the host mafic rocks vary from sharp to gradational. This group of hybrid rock shares border with the mingled rocks, which constitutes the second category of hybrid rock.

b) The mingled rocks are identified by intermingled mafic-felsic zones (Fig. 3d, e). Figure 3 e represents a mingled rock in which the individual mafic and felsic components are clearly visible. The contacts between the felsic and mafic parts are nearly sharp and frequently display cuspate-lobate pattern. At the outcrop scale, presence of cuspate-lobate contacts suggests the effect of magma mingling of coeval mafic and felsic magmas (Barbarin and Didier 1992). Well-defined reaction surfaces can be seen at mafic-felsic contacts in these rocks (Fig. 3f). The reaction surfaces appear to be intermediate in composition between the mafic and felsic endmembers. An important feature observed in this category of hybrid rock at the outcrop scale is the occurrence of veins (Gogoi et al. 2018b). These veins appear to be transporting components or mineral phases from the mafic phase to the felsic phase and vice-versa. Veins occur in the reaction surfaces as well.

c) The third category of hybrid rock occurring in the Ghansura dome is identified as non-porphyritic intermediate rock with emulsions (Fig. 3g). These rocks occupy a small portion of the study domain, sandwiched between the mingled rocks and the porphyritic intermediate rock. The non-porphyritic variant displays a fine comingled texture, where darker mafic phase is suspended in a

fine-grained gray groundmass, forming heterogeneities smaller than a millimeter in size. The mafic emulsions occur as bubble-like heterogeneities ranging from rounded to subrounded in shape.

d) The last category of hybrid rock, which is in contact with the emulsion rock, is the porphyritic intermediate rock. This hybrid rock occupies a significant portion of the Ghansura dome. It appears homogenous in nature, such that individual components of the mafic and felsic magmas could not be traced in this rock. Phenocrysts of plagioclase feldspars are distinctly visible in hand sample. The phenocrysts are set in a fine- to medium-grained gray groundmass giving the rock its characteristic porphyritic nature (Fig. 3h). Another important feature observed in these rocks is the presence of abundant rapakivi feldspars (Fig. 3i). The presence of rapakivi feldspars is considered an important textural feature to characterize hybrid rocks that have formed due to the mixing of compositionally disparate magmas (Hibbard 1991; Baxter and Feely 2002).

Petrography

The rocks of the GRD may be broadly classified into three categories: (a) mafic rocks, representing the mafic endmember, (b) felsic rocks, representing the felsic endmember, and (c) hybrid rocks resulting from the mixing and mingling of a and b, which include mafic rocks containing felsic clasts, mingled rocks, porphyritic rock, and emulsion rock. Sample description and qualitative modal composition are given in Table 1.

Mafic rocks

This rock contains augite, plagioclase, Ti-Fe oxide, and accessory amphibole and biotite. Phenocrysts of augite are observed in thin sections, giving the rock a porphyritic texture. Most of the plagioclase laths are partially or completely engulfed within augite representing sub-ophitic and ophitic texture (Fig. 4a), respectively. Some samples are also depicting a vesicular texture as there are a number of vesicles filled with secondary minerals like chlorite and calcite.

Felsic rocks

The rocks representing the felsic endmember are fine-grained with the mineral grains mostly anhedral in shape (Fig. 4b). The rock dominantly consists of K-feldspar, quartz, and glass with minor amounts of muscovite, iron-oxide, and tourmaline.

Hybrid rocks

Mafic rocks with felsic clasts

In this particular hybrid rock, two types of microzones can be distinguished at crystal scale, one is felsic and the other is mafic, the felsic occurring as small fragments in the mafic (Fig.4c). The felsic zones consist essentially of fine-grained quartz, K-feldspar, muscovite, and biotite with minor amounts of coarser epidote, amphibole, titanite, and iron-oxide. Amphibole mostly occurs at the boundary of the enclaves, where the latter are in contact with the mafic zones. The felsic zones are elongated in a preferred direction with aspect ratios up to 1:10.

The mafic zone consists of amphibole, plagioclase, epidote, titanite, chlorite, quartz, and K-feldspar. Quartz and K-feldspar are not evenly distributed in this zone; rather they are concentrated in discrete patches. The mineral grains are showing a preferred orientation in the direction of the elongation of enclaves.

Mingled rocks

Mingled rocks are fine to medium grained consisting of amphibole, biotite, calcite, quartz, plagioclase, K-feldspar, iron-oxide, titanite, and accessory epidote, chlorite, and muscovite. Two distinct microzones can be identified in thin section: (a) medium-grained mafic zones which consist essentially of amphibole (hereafter referred to as amphibole-rich microzones or ARM) and (b) fine-grained felsic zones consisting of quartz, K-feldspar, iron-oxide, biotite, and accessory amphibole and epidote. These zones are found to be in contact with each other. In the amphibole-rich microzones (ARM), the amphibole at the boundary appears to be optically different than the interior amphibole. Amphibole present in the interior areas are pale green to colorless, whereas those present in the exterior areas show a dark green color (Fig. 4d).

An important feature observed in this particular hybrid rock is the presence of biotite and iron-oxide veins (Fig. 4e). The biotite veins are observed in the felsic zones, which appear to originate from the mafic zones. An interesting feature of the biotite veins is that near the mafic zones where they originate, amphibole constitutes these veins rather than biotite, and as they move away from the mafic zones into the felsic zones, amphibole is replaced by biotite and the veins underwent viscous folding (Fig. 4d). These veins show frequent folding as they traverse across the felsic zones. Veins of iron-oxide are also observed in the felsic zones intruding from the mafic zones. Unlike the biotite veins, veins of iron-oxide are getting dissipated as they move into the felsic zones from the mafic zones instead of flowing as continuous veins in the former. No cross-cutting relationship is observed among these veins indicating their concurrent nature. These veins appear to be

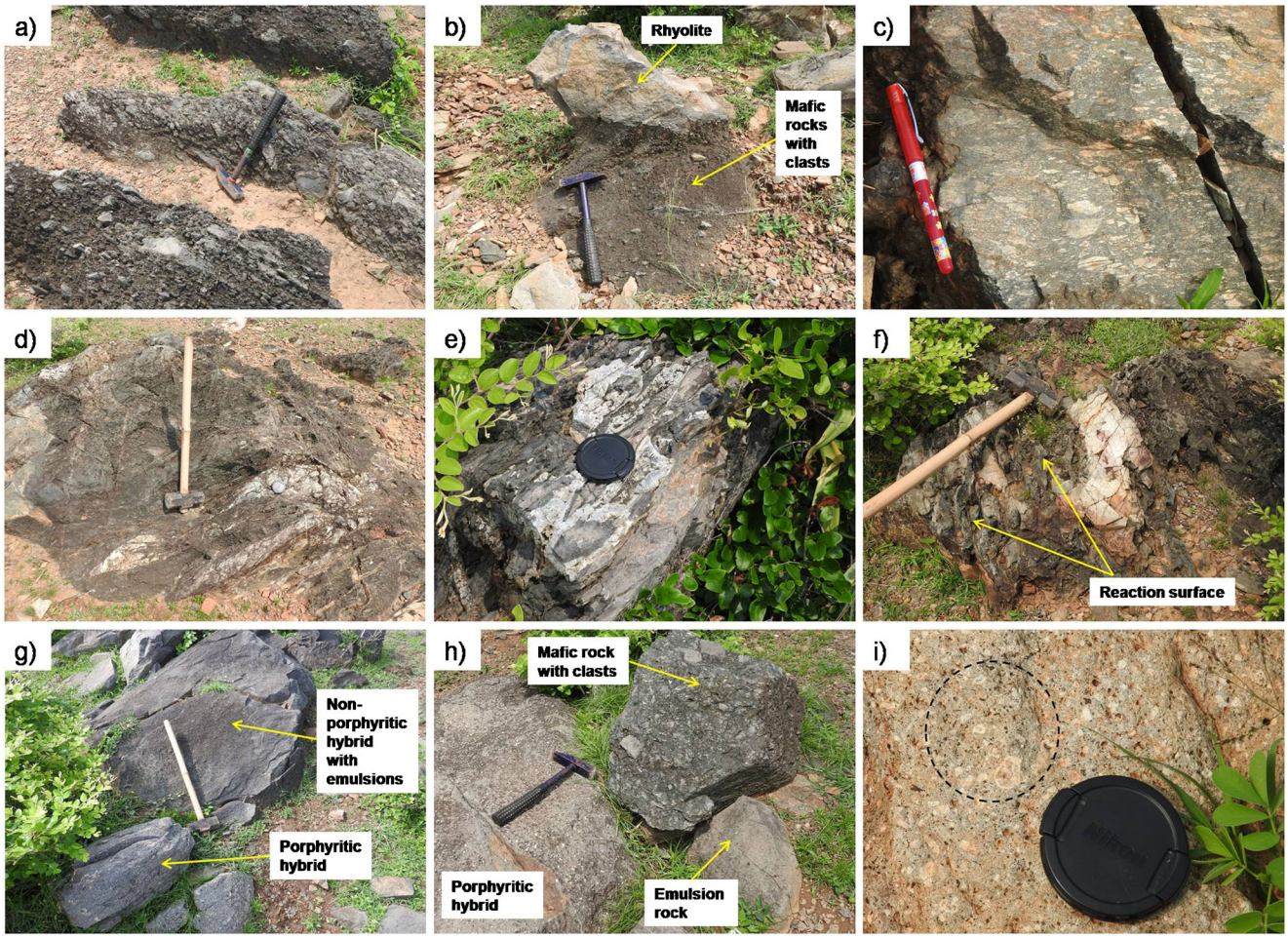

Fig. 3 Field photographs displaying (**a**) mafic rocks containing angular clasts of rhyolite (**b**) contact between rhyolite and mafic rocks with clasts (**c**) felsic clasts, mostly elongated in shape, of various sizes within mafic rock (**d**, **e**). Intermingled mafic-felsic rocks (**f**) reaction surface at mafic-felsic contact (**g**) non-porphyritic hybrid rock with emulsions. The hybrid rock shares well-defined contact with the porphyritic hybrid rock (**h**) porphyritic hybrid rock along with the emulsion rock and mafic rock with clasts (**i**) porphyritic hybrid rock displaying rapakivi texture. A few rapakivi feldspars are seen within the dashed circle

responsible for the enrichment of biotite and iron-oxide in the felsic zones that are transporting these minerals from one zone to another.

Porphyritic rock

This hybrid rock shows holocrystalline and hypidiomorphic texture. Phenocrysts of plagioclase, quartz, and biotite are observed in a fine- to medium-grained groundmass of plagioclase, quartz, K-feldspar, biotite, calcite, apatite, and iron-oxide. Pleochroic halos are observed in biotite, which formed due to the presence of minute radioactive minerals in the biotite grains. Some biotite grains display sagenitic web of titanite needles. Titanite also occurs as inclusions in biotite, which formed due to the alteration of the latter. A number of textures like acicular apatite, quartz ocelli, rapakivi and anti-rapakivi feldspars, feldspars with dissolved core and undissolved rim, and oscillatory zoning in plagioclase are observed in petrographic sections that indicate the hybrid nature of this rock, i.e., this rock formed by the mixing between mafic and felsic magmas (Gogoi et al. 2018b).

An important petrographical feature is observed in this hybrid rock, where smaller-sized plagioclase grains aggregated together to form crystal clusters (Fig. 4f). The plagioclase grains present in these clusters underwent mutual attachment to form phenocrysts of plagioclase (Fig. 4g). This process of crystal aggregation and mutual attachment of mineral grains is termed as synneusis, a term proposed by Vogt (1921). He defined synneusis as the process of swimming together and systematic attachment of crystals suspended in a melt volume. From petrographical observations, it appears that plagioclase crystals aggregated together followed by dissolution of their grain boundaries to form large individual grains of plagioclase. The degree of coalescence varies significantly among the plagioclase grains involved in synneusis. Sometimes, the crystals show aggregation with their grain boundaries intact, while in other cases, there is complete dissolution of grain boundaries to form a larger plagioclase grain. Oscillatory or

Table 1 Sample description and qualitative modal composition

Sample	Major Minerals	Texture	Microstructure
Mafic rocks	Augite (45–55 vol%) Plagioclase (35–40 vol%) Ti-Fe oxide (5–10 vol%)	Porphyritic, ophitic/sub--ophitic, vesicular	
Felsic rocks	Quartz (50–60 vol%) K-feldspar (40–50 vol%)	Fine grained, hypocrystalline	
Mafic rocks with felsic clasts	Amphibole (45–55 vol%) Plagioclase (10–20 vol%) Quartz (10-20 vol%) K-feldspar (5–10 vol%) Biotite (<5 vol%)	Fine to medium grained	Fine-grained felsic clasts are embedded in mafic groundmass. The clasts vary in size from 1mm to a few cm
Mingled rocks	Amphibole (20–30 vol%) Biotite (20–25 vol%) Quartz (10–15 vol%) Plagioclase (10–15 vol%) K-feldspar (5–10 vol%) Iron-oxide (5–10 vol%) Calcite (<5 vol%) Titanite (<5 vol%)	Fine to medium grained	Amphibole-rich microzones (ARM) are observed in thin section. Thin veins of amphibole-biotite and iron-oxide appear to migrate from the ARM into the neighboring felsic zones. The amphibole-biotite veins frequently display viscous folding
Porphyritic rock	Biotite (20–30 vol%) Plagioclase (20–30 vol%) Quartz (20–25 vol%) K-feldspar (15–20 vol%) Calcite (<5 vol%) Iron-oxide (<5 vol%) Apatite (<5 vol%)	Porphyritic, acicular apatite, quartz ocelli, rapakivi and anti-rapakivi feldspars, feldspars with dissolved core and undissolved rim, oscillatory zoned plagioclase	Smaller-sized plagioclase grains have aggregated together to form crystal clusters displaying synneusis
Emulsion rock	Biotite (20–30 vol%) Plagioclase (10–20 vol%) Quartz (10–20 vol%) Amphibole (10–15 vol%) K-feldspar (10–15 vol%) Calcite (<5 vol%) Iron-oxide (<5 vol%) Apatite (<5 vol%)	Acicular apatite, anti-rapakivi feldspars	Spherical to sub-spherical aggregates of amphibole-biotite occur in this rock displaying emulsion texture. The emulsions vary in size from 0.5 to 1 mm in diameter having an average size of around 0.75 mm

other zoning patterns are not observed in the plagioclase crystals associated with synneusis.

Emulsion rock

This hybrid rock is composed of fine- to medium-grained groundmass of plagioclase, biotite, amphibole, quartz, K-feldspar, epidote, calcite, apatite, and iron-oxide. The rock is showing a holocrystalline texture. Amphibole is not evenly distributed in the groundmass; rather it occurs as spherical to subspherical aggregates displaying emulsion texture (Fig. 4h). This variety of hybrid rock displays a fine comingled texture, where one phase is suspended in the other, forming heterogeneities smaller than a millimeter in size. The continuous or coherent phase is represented by crystallized matrix of

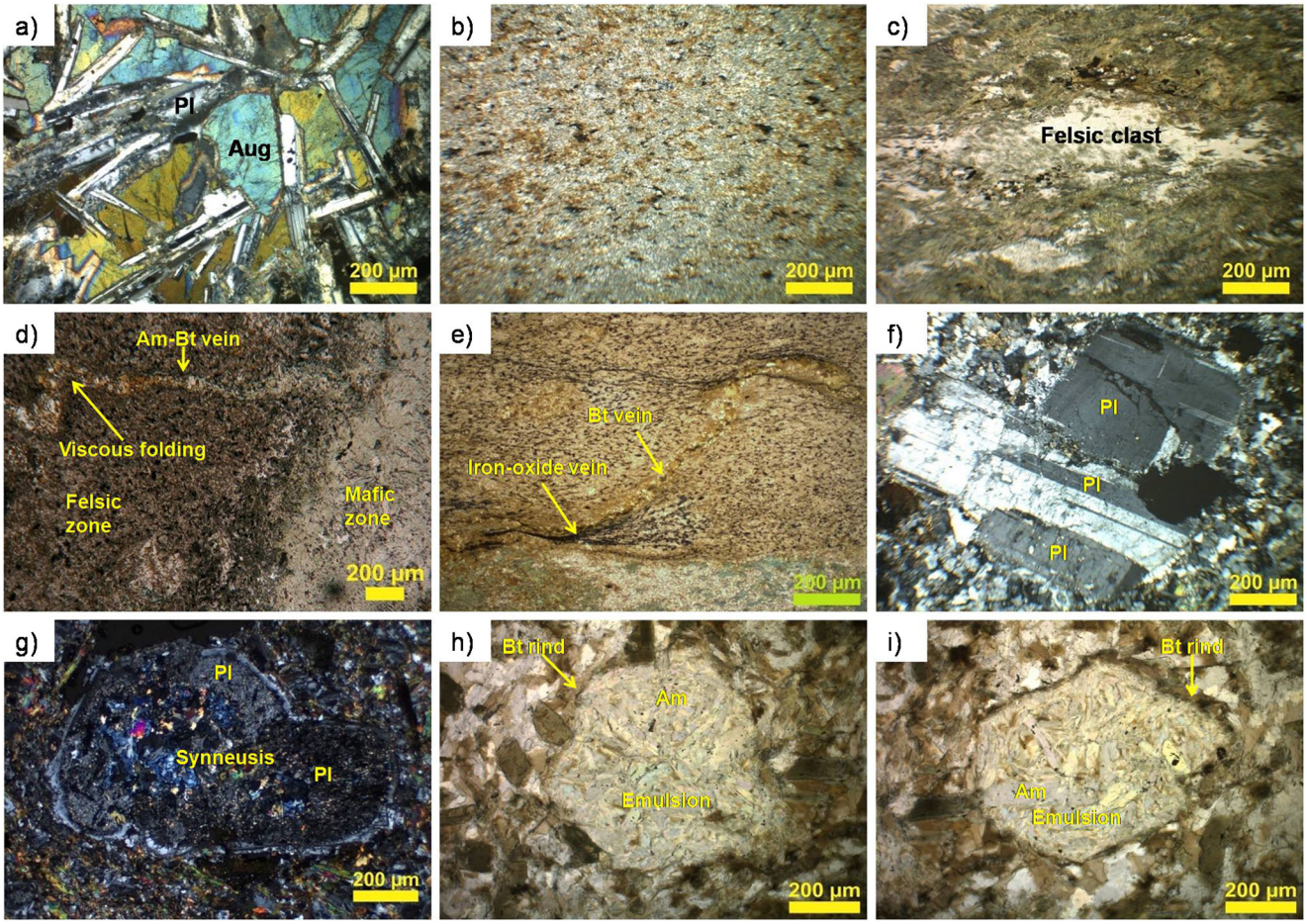

Fig. 4 Photomicrographs displaying (**a**) laths of plagioclase engulfed in augite grains representing ophitic texture in the mafic rocks (**b**) fine-grained felsic groundmass (**c**) a felsic clast occurring in mafic groundmass (**d**) an amphibole-rich microzone (ARM) in contact with felsic zone. The amphiboles constituting the ARM are optically different. The interior amphibole is pale green (actinolite), while the exterior amphibole is green in color (hornblende). An amphibole vein is seen traversing from the mafic zone into the felsic zone. As the vein traverses into the felsic zone, amphibole alters into biotite and the vein undergoes viscous folding (**e**) veins of biotite and iron-oxide traversing from the mafic zone into the felsic zone (**f**) synneusis, in which, smaller-sized plagioclase crystals are aggregating together to form a large crystal cluster (**g**) mutual attachment of two distinct plagioclase crystals involved in synneusis (**h**) an emulsion preserved in the non-porphyritic andesite. The emulsion is dominantly composed of amphiboles having distinct biotite rind (**i**) an amphibole-rich emulsion with distinct biotite rind.

plagioclase, biotite, quartz, K-feldspar, and other accessory minerals, whereas the bubble-like, spherical to subspherical heterogeneities are dominantly composed of amphibole crystals with minor amounts of biotite, which seems to be an altered product of amphibole. The sizes of the bubble-like heterogeneities vary from 0.5 to 1 mm in diameter having an average size of around 0.75 mm. All emulsions are mantled by a distinct biotite rind (Fig. 4i). Magma mixing textures like anti-rapakivi feldspars and acicular apatite are widely distributed in this hybrid rock.

Analytical methods

Mineral chemical analyses were performed using a CAMECA SX 100 electron microprobe at Electron Microprobe Analyzer Laboratory, Geological Survey of India, Faridabad (India) and a CAMECA SX Five instrument at DST-SERB National Facility, Department of Geology (Center of Advanced Study), Institute of Science, Banaras Hindu University (India). The data were obtained using an acceleration voltage of 15 kV, beam current of 10 nA and a beam diameter of ca.1 μm. Standards used includes wollastonite for Si and Ca, periclase for Mg, rhodonite for Mn, albite for Na, corundum for Al, hematite for Fe, orthoclase for K, apatite for P, metallic Cr and Ti for Cr and Ti, halite for Cl, metallic Zn for Zn, fluorite for F, and barite for Ba. The correction applied to the data is that of PAP (Pouchou and Pichoir 1987).

Mineral chemistry

Mineral analyses were carried out on four major mineral phases, i.e., pyroxene, plagioclase, amphibole, and biotite.

We selected these four major minerals for EPMA analyses because of their potential to provide us information on the dynamics of magma mixing between the mafic and felsic magmas. Since these mineral phases are not present in the felsic rocks, mineral chemistry for the felsic endmember is not presented in this work. Moreover, mineral analyses from the felsic rocks and mafic rocks with felsic clasts have not been included in this work due to their little significance in our discussion. Mineral analyses were performed on specific mineral phases from the mafic and hybrid intermediate rocks to understand the mixing process that occurred in the GRD.

Pyroxene

Pyroxene is present exclusively in the mafic rocks. The EPMA data of pyroxene are given in Supplementary Table 1. A total of 8 point data analyses were selected from a number of pyroxene grains present in the mafic samples. All the analyzed pyroxene from the studied samples is classified as Ca-Mg-Fe clinopyroxene and plots in the fields of augite (Fig. 5) based on the classification of Morimoto et al. (1988).

Plagioclase

Plagioclase occurs in the mafic and hybrid rocks of GRD. A total of 16 point data analyses were selected from eight plagioclase grains present in the mafic rocks. The data include core-rim analyses of individual plagioclase grains given in Supplementary Table 2. The compositions of plagioclase for the mafic samples plot in the fields of labradorite and bytownite (Fig. 6a).

Plagioclase analyses were carried out on the hybrid rocks of GRD, which include mingled rocks, porphyritic

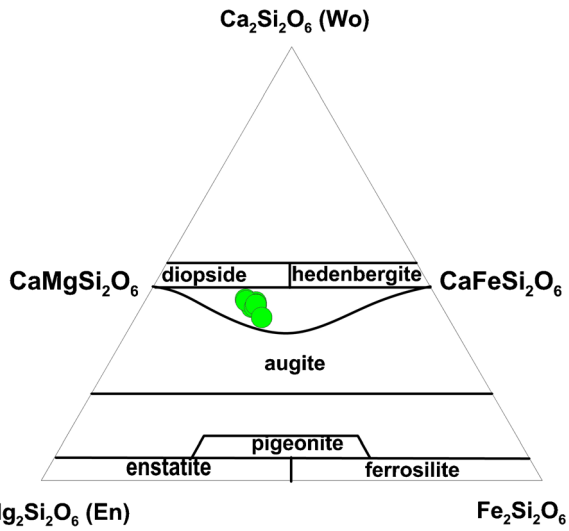

Fig. 5 $Fe_2Si_2O_6$-$Mg_2Si_2O_6$-$Ca_2Si_2O_6$ diagram (Morimoto et al. 1988) showing the composition of pyroxene from the mafic end-member of GRD

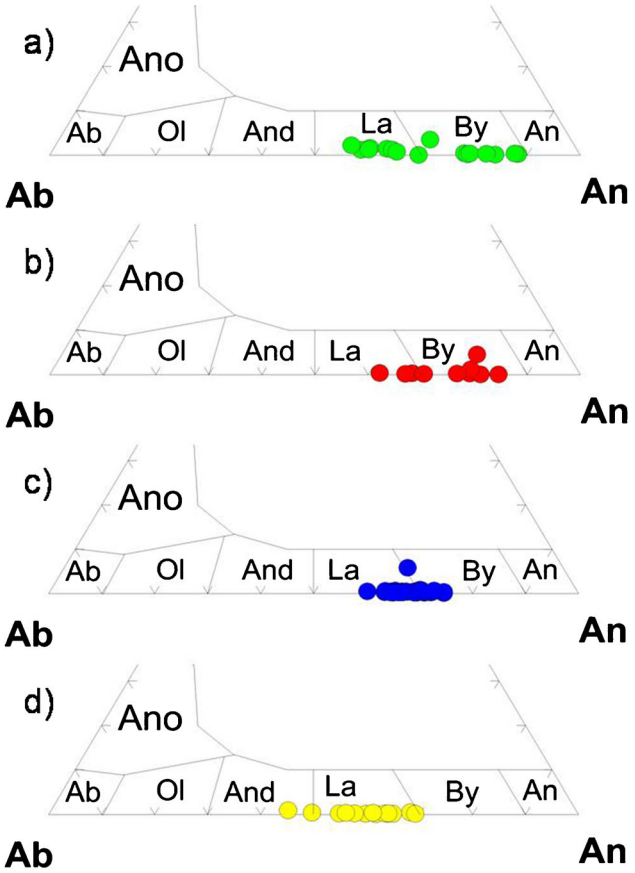

Fig. 6 Nomenclature of plagioclase occurring in the **a** mafic end-member, **b** mingled rocks, **c** porphyritic hybrid rock, and **d** emulsion rock

intermediate rock, and emulsion rock. The representative data of plagioclase from the mingled rocks are provided in Supplementary Table 3. The single point analyses of plagioclase occurring in the ARM of the mingled rocks plot in the fields of labradorite and bytownite (Fig. 6b). Meanwhile, the core-rim analyses of plagioclase crystals involved in synneusis (Supplementary Table 4) in the porphyritic hybrid rock show spike zoning (Fig. 7a, b). Such compositional discontinuities or calcic spikes can be attributed to the process of magma mixing (Hibbard 1991; Baxter and Feely 2002). The compositions of plagioclase plot in the fields of labradorite and bytownite (Fig. 6c) for the porphyritic variant. Furthermore, the representative data of plagioclase for the emulsion rock are provided in Supplementary Table 5, which include single point and core-rim analyses from individual plagioclase grains. The compositions of plagioclase for the emulsion rock plot in the fields of andesine and labradorite (Fig. 6d). The core-rim analyses show normal zoning with Ca-rich cores relative to rims (Fig. 7c, d).

Amphibole

Amphibole occurs as a major mineral phase only in the hybrid rocks of GRD. It is present as an alteration product of

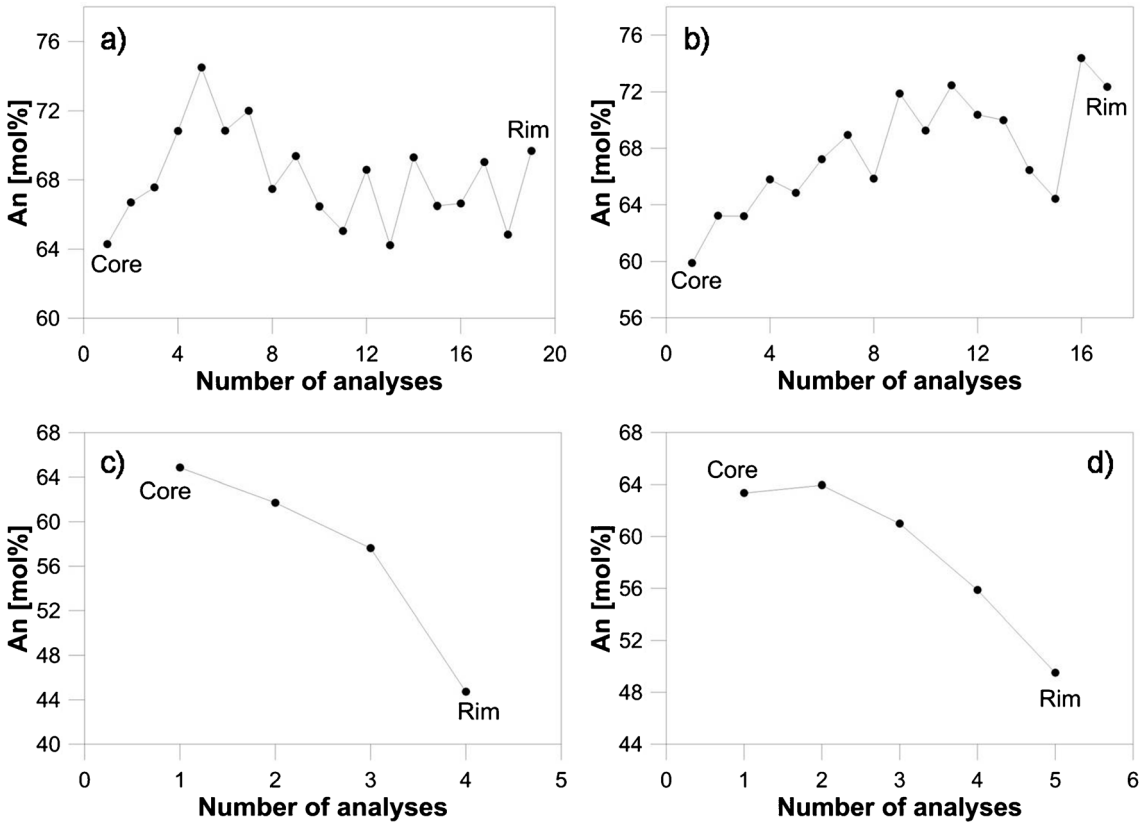

Fig. 7 Anorthite content in mol% of plagioclase crystals **a**, **b** involved in synneusis in the porphyritic hybrid rock showing spike zoning **c**, **d** from the emulsion rock showing normal zoning

clinopyroxene in the mafic endmember, and hence, mineral-chemical data of such amphibole were omitted from this work due to its little significance for further discussion. Amphibole compositions were determined from the hybrid rocks displaying ARM and emulsions with a view to understand the petrogenesis of these rocks. The formulae of amphibole were calculated on the basis of 23 oxygens and amphibole classification was done following Leake et al. (1997).

Representative analyses of amphiboles from the mingled rock displaying ARM are presented in Supplementary Table 6. The compositions of amphiboles were mostly determined for the ARM in this category of hybrid rock. Amphiboles show distinct compositional variation from the interior to the exterior of ARM. Those which are present in the interior are actinolite, whereas those in the exterior zones are hornblende in composition (Fig. 8a).

Amphibole compositions were also analyzed from the hybrid rock displaying emulsion texture. Representative data of amphiboles obtained from the emulsions are presented in Supplementary Table 7. Similar to the hybrid rock displaying ARM, amphiboles display compositional variation from the interior to the exterior of the emulsions. Amphiboles occurring in the interior regions are actinolite in composition, whereas those which are present in the exterior regions are hornblende (Fig. 8b).

Biotite

Biotite occurs as a major mineral phase in the hybrid rocks of GRD. Compositions of biotite were obtained from the mingled rocks, emulsion rock, and porphyritic intermediate rock with a view to understand the mechanisms facilitating magma mixing. The endmember calculation of biotite was done on the basis of 22 oxygen atoms, and Fe^{3+}–Fe^{2+} partitioning from total iron [$FeO_{(t)}$] was carried out following charge balance procedures of Dymek (1983).

Representative data of biotite from the mingled rocks are presented in Supplementary Table 8. Biotite occurring in this hybrid rock plots in the field of siderophyllite (Fig. 9). Biotite compositions were determined from the hybrid rock displaying emulsion texture (Supplementary Table 9). On the Al^{iv} vs. Fe# (Fe/Fe+Mg) classification diagram (Speer 1984), biotite clusters in the field of eastonite and siderophyllite (Fig. 9). Biotite compositions were also determined from the porphyritic intermediate rock. A total of 10 point data analyses were selected from a number of biotite grains present in the hybrid rock sample. The representative data are given in Supplementary Table 10. The compositions of biotite plot in the field of siderophyllite on the Al^{iv} vs. Fe# (Fe/Fe+Mg) classification diagram (Fig. 9). The clustering of biotite compositions from the mingled rocks, emulsion rock,

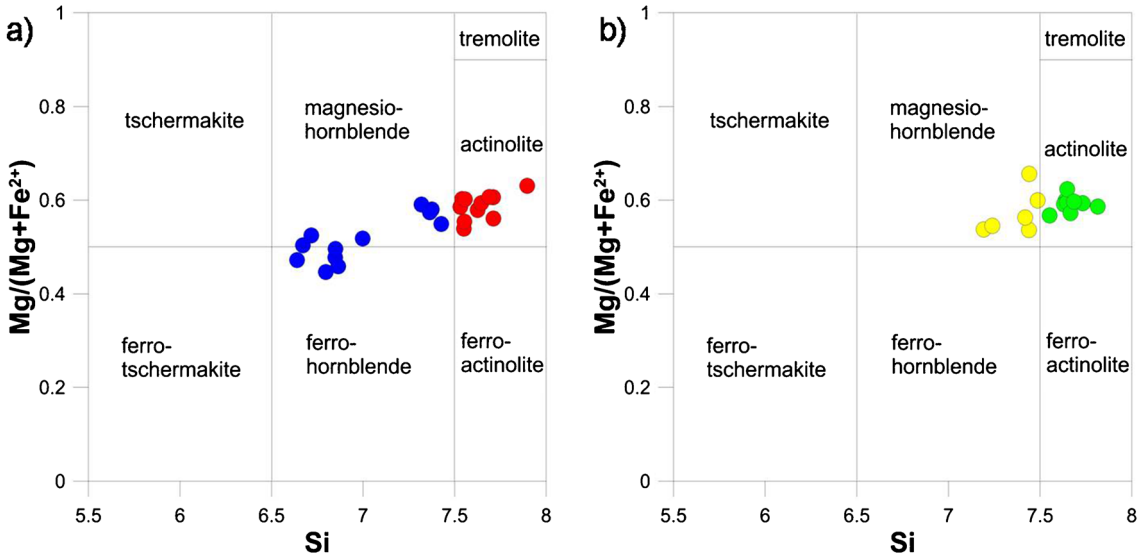

Fig. 8 Nomenclature of amphiboles from the **a** hybrid rock displaying amphibole-rich microzones (ARM). Symbols represent: red circle = ARM interior amphibole and blue circle = ARM exterior amphibole. **b** Hybrid rock with emulsions. Symbols represent: green circle = emulsion interior amphibole and yellow circle = emulsion exterior amphibole.

and porphyritic intermediate rock suggests similar origin for the mineral in these rocks.

Discussion

Crystallization conditions in the magma chamber

Temperature and oxygen fugacity

Previous studies have shown that the Ti content in biotite is directly related to its temperature of crystallization (Patino Douce 1993; Henry et al. 2005). High Ti content corresponds to high temperature of crystallization and vice versa. The Ti and X_{Mg} contents in biotite from the mingled rocks, emulsion rock, and porphyritic rock were plotted in the Ti vs. Mg/(Mg + Fe) diagram (Henry et al. 2005). The Ti-in-biotite geothermometer indicates that most of the biotites in the hybrid rocks crystallized at temperatures estimated to be between 500 and 600 °C (Fig. 10a). Meanwhile, average crystallization temperatures of 1227 °C for clinopyroxene crystallization in the basaltic rocks and 818 °C for amphibole crystallization in the mingled rocks were reported by Gogoi and Saikia (2018a). From the temperature estimates, it can be inferred that interaction of the hotter mafic magma with the colder felsic magma produced a heterogeneous hybrid magma whose temperature was lower than that of the mafic magma. Precursor clinopyroxene originally crystallized in the mafic magma destabilized to amphibole at lower temperatures owing to mixing with the water-rich felsic magma (Castro and Stephens 1992; Choe and Jwa 2004; Ubide et al. 2014). As cooling continued, mafic magma in the hybrid system underwent further hybridization marked by replacement of amphibole with biotite owing to magma mixing.

Compositions of biotite can be utilized to determine the oxygen fugacity conditions that prevailed during magma crystallization. The experimental findings of Wones and Eugster (1965) emphasized the empirical relationship between biotite composition and oxygen fugacity (fO_2), hence making this mineral a valuable tool for redox assessment. In the Fe^{2+}–Fe^{3+}–Mg plot proposed by Wones and Eugster (1965),

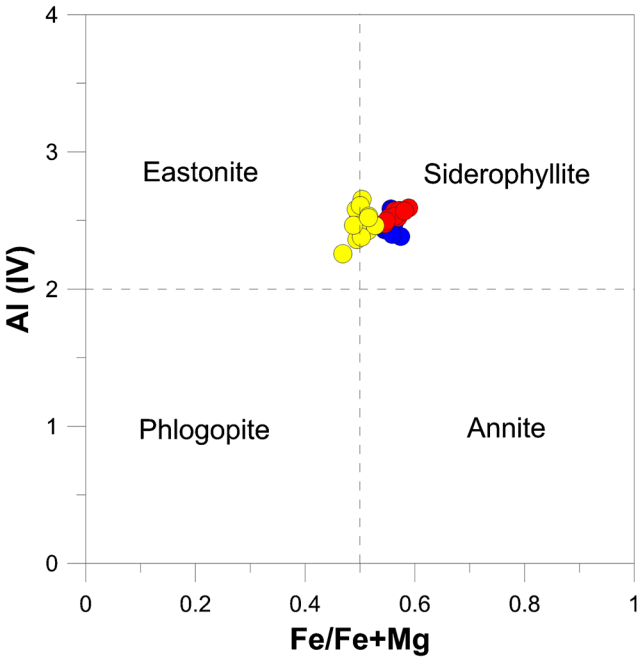

Fig. 9 Nomenclature of biotite from the hybrid rocks. Symbols represent: red circle = biotite from the mingled rocks, yellow circle = biotite from the emulsion rock, and blue circle = biotite from the porphyritic hybrid rock

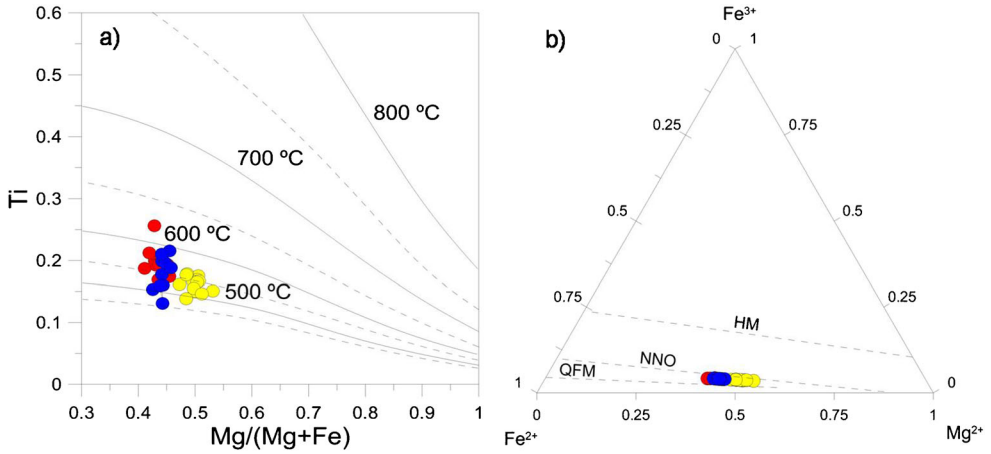

Fig. 10 **a** Ti vs. Mg/(Mg+Fe) plot of biotite from the hybrid rocks (after Henry et al. 2005) illustrating temperatures of biotite formation. **b** Variations of Fe^{2+}–Fe^{3+}–Mg in biotite from the hybrid rocks (after Wones and Eugster 1965). HM, NNO, and QFM represent buffer curves for hematite–magnetite, nickel–nickel oxide, and quartz-fayalite-magnetite buffers, respectively. Symbols represent: red circle = biotite from the mingled rocks, yellow circle = biotite from the emulsion rock, and blue circle = biotite from the porphyritic hybrid rock

compositions of biotite are compared with common oxygen buffers: hematite-magnetite (HM), nickel-nickel oxide (NNO), and quartz-fayalite-magnetite (QFM). The fO_2 of biotite from the hybrid rocks of GRD plots below the NNO and near the QFM buffer (Fig. 10b), indicating that this mineral crystallized under reducing conditions. The reducing nature of the hybrid rocks is also supported by the presence of abundant ilmenite in the mingled rocks (Gogoi et al. 2020c).

Pressure and depth

Biotite compositions can also be used to trace the emplacement and evolutionary history of magmas by estimating the crystallization pressure. There is a strong linear positive relationship between the crystallization pressure (P) and total Al (Al^T) content in biotite (Uchida et al. 2007). An empirical equation to estimate crystallization pressure from total Al content in biotite was introduced:

$$P\ (kbar) = 3.03 \times Al^T – 6.53\ (\pm 0.33) \quad (1)$$

where Al^T is the total Al content in biotite (calculated on the basis of 22 oxygens).

Using Equation 1, the estimated pressures for the mingled rocks range from 2.49 to 3.13 kbar (average = 2.79 kbar; Supplementary Table 8), pressures for the emulsion rock range from 1.89 to 3.2 kbar (average = 2.68 kbar; Supplementary Table 9) and pressures for the porphyritic hybrid rock range from 2.31 to 3.58 kbar (average = 2.86 kbar; Supplementary Table 10). From the calculated pressures, it can be estimated that the GRD was emplaced at a depth of around 9–10 km. The average pressure derived from the biotite geobarometer is consistent with the average pressure (2.77 kbar) reported by Gogoi and Saikia (2018a) for GRD, which was calculated using the Al-in-hornblende barometer of Anderson and Smith (1995).

Genesis of the mafic rocks with felsic clasts

The mafic rocks with felsic clasts contain abundant felsic rock fragments embedded in a mafic groundmass. These fragments are essentially fine-grained and resemble the felsic rocks occurring in the GRD. A large number of these rock fragments show reaction surfaces suggesting limited chemical interaction with the surrounding mafic phase (Gogoi et al. 2018b). The nature of interaction between the felsic clasts and mafic phase is restricted to chemical diffusion and mechanical transfer of crystals. The felsic and mafic domains are distinctly preserved in this category of hybrid rocks indicating magma mingling rather than mixing. From field and petrographical observations, it appears that solidification had already begun in the host felsic magma chamber when invading mafic magma disrupted it. The intrusion disrupted the already solidified zone of the magma chamber leading to the formation of abundant felsic clasts. These clasts were then assimilated by the intruding mafic magma, which are now preserved as rock fragments.

Genesis of the mingled rocks displaying viscous folding

The mingled rocks are the products of magma mingling rather than mixing as individual mafic and felsic components are easily distinguishable in these rocks (Fig. 3d, e, f). Unlike mixing, magma mingling is a process where coeval magmas of different compositions come into contact but do not mix or blend. The resultant product is a heterogeneous mixture containing discrete portions of the endmember magmas (e.g.,

basalt and rhyolite). Mineral transporting veins extensively occur in this hybrid rock that appears to be distributing mineral phases from the mafic components to the felsic components and vice versa. The widespread occurrence of veins suggests that when mafic magma invaded the felsic magma chamber, the two contrasting melts tried to mix so as to attain an equilibrium condition. The veins act as conduits for exchange of components or mineral phases between the two contrasting magmas (Gogoi et al. 2018b).

The mingled rocks of our study area preserve ARM. Earlier works on ARM (Castro and Stephens 1992; Sial et al. 1998; Janoušek et al. 2000; Stephens 2001; Choe and Jwa 2004; Martin 2007; Ubide et al. 2014) inferred that these monomineralic zones form from solid state reaction of earlier clinopyroxene crystals. Petrographic evidence suggests that ARM replaced precursor clinopyroxene that initially crystallized in the mafic magma and disintegrated to amphibole owing to interaction with the felsic, water-rich magma (Castro and Stephens 1992; Choe and Jwa 2004; Ubide et al. 2014). This is evident from the compositional variations of amphibole across the ARM (Fig. 8a), which indicates that the crystallizing mafic magma was interacting with the adjacent felsic magma (Gogoi and Saikia 2018a). The formation of amphibole grains in the mafic system facilitated the mechanical transfer of crystals from the mafic phase to the felsic phase, which was in all probability a crystal-poor fluid. The amphibole-biotite veins are bearers of the crystal transfer mechanism that facilitated mixing between two rheologically contrasting magmas in our study area.

An interesting feature displayed by the amphibole-biotite veins is viscous folding (Fig. 4d). Viscous folding is a fluid instability that can facilitate mixing between two magmas with pronounced viscosity contrast (Gogoi and Saikia 2018a, Gogoi et al. 2020b). Buckling or folding instability occurs when a thin thread of a higher viscosity fluid treads into a lower viscosity fluid (Cubaud and Mason 2006a, b, 2007, 2008; Chung et al. 2010; Darvishi and Cubaud 2012). In our scenario, the amphibole-biotite veins are depicting viscous folding. In other words, the viscosity of the mafic magma was much larger than the felsic magma. This condition is only possible when the former is crystal-rich and the latter is crystal-poor. When crystal-rich mafic magma veined into the felsic melt, the former experienced compressional stress owing to viscosity difference between the two mediums and underwent folding in order to reduce dissipation and conserve mass. Folding reduced the velocity of the mafic phase and the sinuous shape of the veins increased the interfacial area between the two disparate phases. The felsic melt got trapped between the folds of the mafic phase enhancing chemical diffusion and mixing between the two magmas.

Genesis of the non-porphyritic intermediate rock displaying emulsion texture

The non-porphyritic intermediate rock of the GRD displays emulsion texture. The emulsion texture is a co-mingled texture that is characterized by roundish bodies of one component (dispersed phase) suspended in the other coherent component (continuous phase) (Freundt and Schmincke 1992). The emulsions observed in this variety of hybrid rock are dominantly composed of amphibole and minor biotite with well-developed biotite rinds. From petrographic observations, it appears that the biotite rinds on the mafic emulsions were probably formed due to chemical interaction between the amphibole-rich emulsions and K-rich felsic magma (Farner et al. 2014; Ubide et al. 2014). This is also supported by the compositional variations of amphibole across the emulsions (Fig. 8b).

From petrographical and mineral-chemical analyses, we infer that when mafic magma, containing phenocrysts of augite, came in contact with felsic magma, diffusion of volatiles, H^+ and Al^{3+} ions, occurred from the felsic to the mafic system. These cations reacted with the clinopyroxene phenocrysts in the mafic magma to form amphibole crystals, which in turn, greatly increased the viscosity of the mafic system. After their formation, the amphibole crystals ventured into the adjacent felsic magma as veins. As these veins traversed in the felsic medium, they underwent sinuous perturbations as a result of the competition between the viscous torque, due to difference in drag on each side of the veins, and the dynamic viscous bending resistance (Cubaud and Mason 2009). Further downstream, the undulations amplified and swirls started to develop on the sinuous veins by accumulating the high viscosity mafic phase into central bulbs and depleting the regions in between them forming tails. Gradually the tails thinned out and blended into the surrounding felsic melt forming discrete viscous emulsions/swirls. The formation of viscous swirls resulted in the formation of large new surface area, which ultimately led to enhanced chemical diffusion and mixing (Richards et al. 1994; Gogoi and Saikia 2019). It has to be noted here that emulsions preserved in magmatic rocks may reflect earlier drops of fluid or melt suspended into silicate melt (Davidson and Kamenetsky 2007; Agangi and Reddy 2016). However, amphibole-rich emulsions encountered in the non-porphyritic intermediate rock share textural resemblance with amphibole-biotite clots reported in a number of magma mixing studies (Castro and Stephens 1992; Janoušek et al. 2000; Choe and Jwa 2004; Ubide et al. 2014). These studies have attributed the formation of these clots to replacement of early-formed clinopyroxene phenocrysts by amphibole-biotite aggregates, possibly as a result of re-equilibration during magma mixing. As such, we do not agree that emulsions in our studied rocks are melt suspensions.

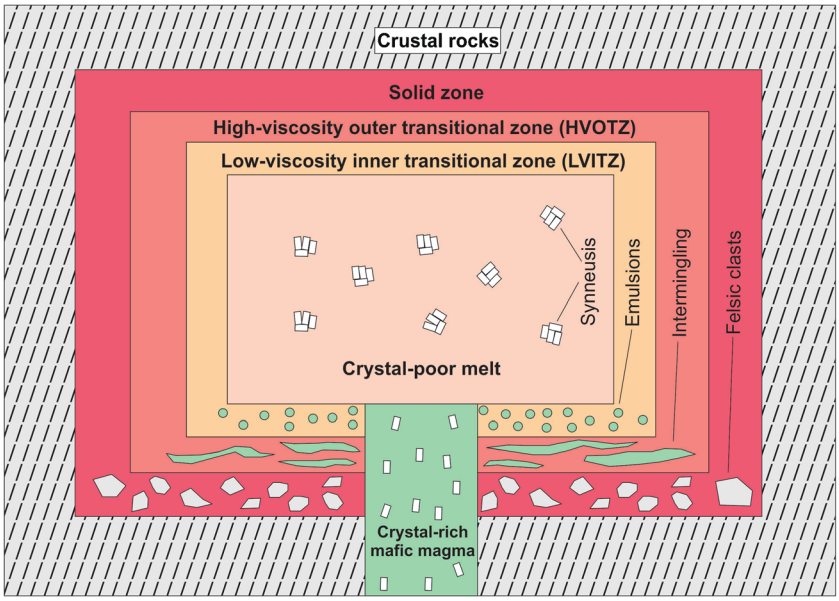

Fig. 11 A schematic diagram showing the nature of the subvolcanic felsic magma chamber representing the GRD when crystal-rich mafic magma intruded it. The GRD was a zoned magma chamber having temperature induced physical boundary layers with varying viscosities when mafic magma intruded it. The outermost zone was completely solid now preserved as clasts in the mafic rocks. The innermost zone was completely melt, having least viscosity, that interacted with the mafic magma forming porphyritic hybrid rocks displaying synneusis. Between these two zones, there were two transitional zones—the High-Viscosity Outer Transitional Zone (HVOTZ) that was in contact with the solid zone and the Low-Viscosity Inner Transitional Zone (LVITZ) that was in contact with the melt. Depending upon the viscosity regime, mafic magma interacted with the felsic magma to generate viscous folding in the HVOTZ, while in the LVITZ formation of emulsions was favored to facilitate the mixing process

Genesis of the porphyritic intermediate rock displaying synneusis

The porphyritic intermediate rock of GRD preserves synneusis, in which smaller crystals of plagioclase have aggregated together to form larger crystals or phenocrysts giving the rock its characteristic porphyritic nature. From field, petrographical, and mineral chemical observations, it is inferred that a certain portion of the felsic magma chamber was entirely melt when mafic magma intruded it. This melt zone interacted with the mafic magma to form the porphyritic intermediate rock. The homogenous nature of this rock suggests that they have formed due to well mixing of the two contrasting magmas. The preservation of synneusis in the hybrid rock indicates that crystals drifted in a melt volume and mutually attached together to form larger crystals or phenocrysts. The indistinguishable compositions of plagioclase from the mafic and the porphyritic intermediate rocks strongly indicate that plagioclase crystals occurring in the hybrid rock were supplied by the mafic magma. Based on these observations, it is inferred that the mafic magma was crystal-rich when it intruded the felsic magma chamber. The crystal-rich nature of the mafic magma is evident from the porphyritic and coarse-grained nature of the mafic rocks. After intrusion, the crystals of the mafic magma were dispersed into the melt zone of the felsic reservoir. The crystal-poor nature of the melt zone within the felsic magma chamber allowed the plagioclase crystals of the mafic endmember to drift and accumulate together to form larger crystals, resulting in an intermediate hybrid rock of porphyritic nature (Gogoi and Saikia 2018b).

Magma chamber dynamics

The GRD presents an ideal geological setting where study of magma mixing dynamics can significantly contribute toward understanding the geodynamics of a subvolcanic magma chamber. Field observations clearly indicate that mafic magma made its way through the already solidified portion of the felsic magma chamber and interacted with the remaining melt to form a wide variety of hybrid rocks (Fig. 3). From the above discussion, it is quite evident that the GRD was a zoned magma chamber that consisted of rheologically contrasting magmatic layers. A certain portion of the magma chamber, possibly the outermost zone, was completely solid as indicated by the occurrence of mafic rocks with felsic clasts. On the other hand, a certain portion of the magma chamber, possibly the innermost zone, was entirely melt as indicated by the presence of porphyritic intermediate rock displaying synneusis. Between these two zones, there were two transitional zones—the High-Viscosity Outer Transitional Zone (HVOTZ) that was in contact with the solid zone and the Low-Viscosity Inner Transitional Zone (LVITZ) that was in contact with the melt. The intruding mafic magma interacted with the HVOTZ to form mingled rocks that preserve ARM and viscous folding. On the other hand, the mafic magma interacted with the LVITZ to form the non-porphyritic intermediate rock displaying

emulsion texture. The contact between the porphyritic and non-porphyritic intermediate rocks is very well demarcated in the field (Fig. 3g). Darvishi and Cubaud (2012) proposed that emulsification of a high-viscosity fluid propagating through a low-viscosity fluid in microgeometries is facilitated at fast flow rates. In our magma mixing scenario, the mineral transporting veins could flow at fast rates when the viscosity of the felsic medium was low. Hence, the magmatic layer within the felsic magma chamber that was involved in the formation of the non-porphyritic intermediate rock with emulsions had low viscosity, and correspondingly the magmatic layer that facilitated the formation of mingled rocks displaying viscous folding had higher viscosity. Thus, the GRD was a zoned magma chamber having temperature induced physical boundary layers with varying viscosities when mafic magma intruded it (Fig. 11). The outermost zone was completely solid now preserved as felsic clasts in the mafic rocks. The innermost zone was completely melt, having least viscosity, that interacted with the mafic magma forming porphyritic hybrid displaying synneusis. Between these two zones, there existed two transitional zones, i.e., the HVOTZ and the LVITZ.

Conclusions The GRD was a zoned magma chamber having temperature induced physical boundary layers with varying viscosities when mafic magma intruded it. The outermost zone was completely solid now preserved as felsic clasts in the mafic rocks. The innermost zone was completely melt, having least viscosity, that interacted with the intruding mafic magma forming porphyritic intermediate rock displaying synneusis. The compositions of plagioclase involved in synneusis are similar to that of the mafic endmember. Between these two zones, there were two transitional zones—the HVOTZ that was in contact with the solid zone and the LVITZ that was in contact with the melt. When mafic magma, containing phenocrysts of augite, came in contact with felsic magma, diffusion of cations like H^+ and Al^{3+} occurred from the felsic to the mafic system. These cations reacted with the augite phenocrysts in the mafic magma to form amphibole crystals, which greatly increased the viscosity of the mafic system. The formation of amphibole grains in the mafic system facilitated the mechanical transfer of crystals allowing amphibole crystals to flow into the adjacent felsic magma as veins. Depending upon the viscosity regime, the veins underwent viscous folding in the HVOTZ, while in the LVITZ, formation of emulsions was favored to facilitate the mixing process.

Supplementary Information The online version contains supplementary material available at https://doi.org/10.1007/s12517-021-08140-w.

Acknowledgements We would like to express our sincere gratitude to the anonymous reviewers for their insightful and constructive comments. The authors acknowledge the CSIR grant vide Project no. 24(0317)/12/EMR-II. Bibhuti Gogoi acknowledges the CSIR JRF/SRF fellowship no. 09/045(1146)/2011-EMR-I. The authors are grateful to their supervisor, Dr. Ashima Saikia, for the geochemical data used in this work. The authors are also grateful to Professor NV Chalapathi Rao and Dr. Dinesh Pandit for EPMA analyses at DST-SERB National Facility, Department of Geology (Center of Advanced Study), Institute of Science, Banaras Hindu University.

Declarations

Conflict of interest The authors declare that they have no competing interests.

References

Acharyya SK (2003) The nature of Mesoproterozoic central Indian tectonic zone with exhumed and reworked older granulites. Gondwana Res 6:197–214

Agangi A, Reddy SM (2016) Open-system behaviour of magmatic fluid phase and transport of copper in arc magmas at Krakatau and Batur volcanoes, Indonesia. J Volcanol Geotherm Res 327:669–686

Agangi A, McPhie J, Kamenetsky VS (2011) Magma chamber dynamics in a silicic LIP revealed by quartz: the Mesoproterozoic Gawler Range Volcanics. Lithos 126(1-2):68–83

Ahmad M, Dubey J (2011) Report on prospecting for gold and silver mineralization in Munger Rajgir group of rocks in Nalanda district, Bihar. P(ii), Unpublished report, GSI (F.S.: 2008-09, 2009-10, 2011-12)

Ahmad M, Paul AQ (2013) Investigation of volcano-sedimentary sequence and associated rocks to identify gold and base metal mineralization at Gere-Kewti Area of Gaya District, Bihar (G4). Unpublished Report Geological Society of India, Bangalore

Ahmad M, Wanjari N (2009) Volcano-sedimentary sequence in the Munger-Rajgir metasedimentary belt, Gaya district, Bihar. Ind J Geosci 63:351–360

Ahmad M, Paul AQ, Negi P, Akhtar S, Gogoi B, Saikia A (2021) Mafic rocks with back-arc E-MORB affinity from the Chotanagpur Granite Gneiss Complex of India: relicts of a Proterozoic Ophiolite suite. In: Geological Magazine, pp 1–16. https://doi.org/10.1017/S0016756821000078

Anderson JL, Smith DR (1995) The effects of temperature and fO_2 on the Al-in hornblende barometer. Am Mineral 8:549–559

Aref H, El Naschie MS (1995) Chaos applied to fluid mixing. Pergamon Press Reprinted from Chaos, Solutions and Fractals 4 Exeter

Bachmann O, Bergantz GW (2004) On the origin of crystal-poor rhyolites: extracted from batholithic crystal mushes. J Petrol 45:1565–1582

Barbarin B, Didier J (1992) Genesis and evolution of mafic microgranular enclaves through various types of interaction between coexisting felsic and mafic magmas. Trans Roy Soc Edinb Earth Sci 83:145–153

Baxter S, Feely M (2002) Magma mixing and mingling textures in granitoids: examples from the Galway Granite, Connemara, Ireland. Mineral Petrol 76:63–74

Castro A, Stephens WE (1992) Amphibole-rich polycrystalline clots in calc-alkaline granitic rocks and their enclaves. Can Mineral 30:1093–1112

Charreteur G, Tegner C (2013) Magmatic emulsion texture formed by mixing during extrusion, Raudafell composite complex, Breiddalur volcano, eastern Iceland. Bull Volcanol 75:721

Chatterjee N, Ghose NC (2011) Extensive Early Neoproterozoic high-grade metamorphism in North Chotanagpur Gneissic Complex of the Central Indian Tectonic Zone. Gondwana Res 20:362–379

Choe WH, Jwa YJ (2004) Petrological and geochemical evidences for magma mixing in the Palgongsan Pluton. Geosci J 8(4):343–354
Chung C, Choi D, Kim JM, Ahn KH, Lee SJ (2010) Numerical and experimental studies on the viscous folding in diverging microchannels. Microfluid Nanofluid 8:767–776
Cubaud T, Mason TG (2006a) Folding of viscous threads in diverging microchannels. Phys Rev Lett 96:114501
Cubaud T, Mason TG (2006b) Folding of viscous threads in microfluidics. Phys Fluids 18:091108
Cubaud T, Mason TG (2007) Swirling of viscous fluid threads in microchannels. Phys Rev Lett 98:264501
Cubaud T, Mason TG (2008) Formation of miscible fluid microstructures by hydrodynamic focusing in plane geometries. Phys Fluids 20: 053302
Cubaud T, Mason TG (2009) High-viscosity fluid threads in weakly diffusive microfluidic systems. New J Phys 11:075029
Darvishi S, Cubaud T (2012) Formation of capillary structures with highly viscous fluids in plane microchannels. Soft Matter 8:10658
Davidson P, Kamenetsky VS (2007) Primary aqueous fluids in rhyolitic magmas: melt inclusion evidence for pre- and post-trapping exsolution. Chem Geol 237:372–383
De Campos CP, Perugini D, Ertel-Ingrisch W, Dingwell DB, Poli G (2011) Enhancement of magma mixing efficiency by chaotic dynamics: an experimental study. Contrib Mineral Petrol 161:863–881
DePaolo DJ (1981) Trace-element and isotopic effects of combined wallrock assimilation and fractional crystallization. Earth Planet Sci Lett 53:189–202
Dymek RF (1983) Titanium, aluminum and interlayer cation substitutions in biotite from high-grade gneisses, west Greenland. Am Mineral 68(9–10):880–899
Farner MJ, Lee CTA, Putrika KD (2014) Mafic-felsic magma mixing limited by reactive processes: a case study of biotite-rich rinds on mafic enclaves. Earth Planet Sci Lett 393:49–59
Farrell J, Smith RB, Husen S, Diehl T (2014) Tomography from twenty-six years of seismicity reveals the spatial extent of the Yellowstone crustal magma reservoir extends well beyond the Yellowstone caldera. Geophys Res Lett 41:3068–3073. https://doi.org/10.1002/2014GL059588
Freundt A, Schmincke HU (1992) Mixing of rhyolite, trachyte and basalt magma erupted from a vertically and laterally zoned reservoir, composite flow P1, Gran Canaria. Contrib Mineral Petrol 112:1–19
Gogoi B, Saikia A (2018a) Role of viscous folding in magma mixing. Chem Geol 501:26–34
Gogoi B, Saikia A (2018b) Synneusis: does its preservation imply magma mixing? Mineralogia 49:99–117
Gogoi B, Saikia A (2019) The genesis of emulsion texture owing to magma mixing in Ghansura Felsic Dome of Chotanagpur Granite Gneiss Complex of Eastern India. Can Mineral 57:311–338
Gogoi B, Saikia A, Ahmad M (2017) Titanite-centered ocellar texture: a petrological tool to unravel the mechanism enhancing magma mixing. Period Mineral 86:245–273
Gogoi B, Saikia A, Ahmad M (2018a) Field evidence, mineral chemical and geochemical constraints on mafic-felsic magma interactions in a vertically zoned magma chamber from the Chotanagpur Granite Gneiss Complex of Eastern India. Chem Erde 78:78–102
Gogoi B, Saikia A, Ahmad M, Ahmad T (2018b) Evaluation of magma mixing in the subvolcanic rocks of Ghansura Felsic Dome of Chotanagpur Granite Gneiss Complex, eastern India. Mineral Petrol 112:393–413
Gogoi B, Saikia A, Ahmad M (2020a) Mafic-felsic magma interactions in the Bathani volcanic-plutonic complex of Chotanagpur Granite Gneiss Complex, eastern India: implications for assembly of the Greater Indian Landmass during the Proterozoic. Episodes 43(2): 785–810
Gogoi B, Chauhan H, Hazarika G, Baruah A, Saikia M, Hazarika PJ (2020b) Significance of viscous folding in the migmatites of Chotanagpur Granite Gneiss Complex, eastern India. Earth Env Sci Trans Roy Soc Edinb 111:119–134. https://doi.org/10.1017/S1755691020000067
Gogoi B, Chauhan H, Saikia A (2020c) Viscous dilation as a mechanism of magma mixing in the Ghansura Rhyolite Dome of Bathani volcano-sedimentary sequence, Eastern India. Period Mineral 89: 285–295
Grove TL, Kinzler RJ, Baker MB, Donelly-Nollan JM, Lesher CE (1988) Assimilation of granite by basaltic magma at Burnt Lava Flow, Medicine Lake Volcano, Northern California, decoupling of heat and mass-transfer. Contrib Mineral Petrol 99:320–343
Hawkesworth CJ, Blake S, Evans P, Hughes R, Macdonald R, Thomas LE, Turner SP, Zellmer G (2000) Time scales of crystal fractionation in magma chambers. Integrating physical, isotopic and geochemical perspectives. J Petrol 41:991–1006
Henry DJ, Guidotti CV, Thomson JA (2005) The Ti-saturation surface for low to medium pressure metapelitic biotite: implications for geothermometry and Ti-substitution mechanisms. Am Mineral 90: 316–328
Hibbard MJ (1981) The magma mixing origin of mantled feldspars. Contrib Mineral Petrol 76:158–170
Hibbard MJ (1991) Textural anatomy of twelve magma-mixed granitoid systems. In: Didier J, Barbarin B (eds) Enclaves and granite petrology. Developments in petrology. Elsevier, Amsterdam, pp 431–444
Hildreth W, Wilson CJN (2007) Compositional zoning of the Bishop Tuff. J Petrol 48:951–999
Huppert HE, Turner JS, Stephen R, Sparks J (1982) Replenished magma chambers; effects of compositional zonation and input rates. Earth Planet Sci Lett 57:345–357
Janoušek V, Bowes DR, Braithwaite CJR, Rogers G (2000) Microstructural and mineralogical evidence for limited involvement of magma mixing in the petrogenesis of a Hercynian high-K calc-alkaline intrusion: the Kozarovice granodiorite, Central Bohemian Pluton, Czech Republic. Trans Roy Soc Edinb Earth Sci 91:15–26
Leake BE, Woolley AR, Arps CES, Birch WD, Gilbert MC, Grice JD, Howthorne FC, Kato A, Kisch HJ, Krivovichev VG, Linthout K, Laird J, Mandarino JA (1997) Nomenclature of amphiboles. Report of the subcommittee on amphiboles of the International Mineralogical Association: commission on new mineral names. Mineral Mag 61:295–321
Lowenstern JB, Smith RB, Hill DP (2006) Monitoring super-volcanoes: geophysical and geochemical signals at Yellowstone and other large caldera systems. Philos Trans R Soc London Ser A 364:2055–2072
Martin RF (2007) Amphiboles in the Igneous Environment. Rev Mineral Geochem 67:323–358
McBirney AR (1980) Mixing and unmixing in magmas. J Volcanol Geotherm Res 7:357–371
Morimoto N, Fabries J, Ferguson AK, Ginzburg IV, Ross M, Seifert FA, Zussman J, Aoki K, Gottardi G (1988) Nomenclature of pyroxenes. Am Mineral 73:1123–1133
Ottino JM (1989) The mixing of fluids. Sci Am 260:56–67
Patino Douce AE (1993) Titanium substitution in biotite: an empirical model with applications to thermometry, O_2 and H_2O barometries, and consequences for biotite stability. Chem Geol 108:133–162
Perugini D, Poli G (2012) The mixing of magmas in plutonic and volcanic environments: Analogies and differences. Lithos 153:261–277
Perugini D, Poli G, Gatta G (2002) Analysis and simulation of magma mixing processes in 3D. Lithos 65:313–330
Pouchou JL, Pichoir F (1987) Basic expressions of PAP computation for quantitative EPMA. Proceedings of ICXOM 11, Ontario, pp 249–253
Renjith ML, Charan SN, Subbarao DV, Babu EVSSK, Rajashekhar VB (2014) Grain to outcrop-scale frozen moments of dynamic magma mixing in the syenite magma chamber, Yelagiri Alkaline Complex, South India. Geosci Front 5(6):801–820

Richards JR, Lenhoff AM, Beris AN (1994) Dynamic breakup of liquid-liquid jets. Phys Fluids A 6:2640–2655

Romero AE, McEvilly TV, Majer EL, Michelini A (1993) Velocity structure of the Long Valley caldera from the inversion of local earthquake P-travel and S-travel times. J Geophys Res 98:19,869–19,879

Saikia A, Gogoi B, Ahmad M, Ahmad T (2014) Geochemical constraints on the evolution of mafic and felsic rocks in the Bathani volcanic and Volcanosedimentary sequence of Chotangpur Granite Gneiss Complex. J Earth Syst Sci 123:959–987

Saikia A, Gogoi B, Kaulina T, Lialina L, Bayanova T, Ahmad M (2017) Geochemical and U–Pb zircon age characterization of granites of the Bathani Volcano Sedimentary sequence, Chotanagpur Granite Gneiss Complex, eastern India: vestiges of the Nuna supercontinent in the Central Indian Tectonic Zone. In: Pant NC, Dasgupta S (eds) Crustal Evolution of India and Antarctica: The Supercontinent Connection, vol 457. Geological Society, London, Special Publications, pp 233–252

Saikia A, Gogoi B, Ahmad M, Kumar R, Kaulina T, Bayanova T (2019) Mineral Chemistry, Sr-Nd Isotope Geochemistry and Petrogenesis of the Granites of Bathani Volcano-Sedimentary Sequence from the Northern Fringe of Chotanagpur Granite Gneiss Complex of Eastern India. In: Mondal M (ed) Geological Evolution of the Precambrian Indian Shield, Society of Earth Scientists Series. Springer, Cham, pp 79–120

Sial AN, Ferreira VP, Fallick AE, Cruz MJM (1998) Amphibole-rich clots in calc-alkalic granitoids in the Borborema province, northeastern Brazil. J S Am Earth Sci 11:457–471

Singer BS, Andersen NL, Le Mével H et al (2014) Dynamics of a large, restless, rhyolitic magma system at Laguna del Maule, southern Andes, Chile. GSA Today 24:4–10

Snyder D (1997) The mixing and mingling of magmas. Endeavour 27: 19–22

Sosa-Ceballos G, Gardner JE, Siebe C, Macías JL (2012) A caldera-forming eruption ~14100 ^{14}C yr BP at Popocatépetl volcano, México. Insights from eruption dynamics and magma mixing. J Volcanol Geotherm Res 212-213:27–40

Sparks RS, Sigurdsson H, Wilson L (1977) Magma mixing: a mechanism for triggering acid explosive eruptions. Nature 267:315–317

Speer JA (1984) Micas in igneous rocks. Rev Mineral Geochem 13:299–356

Spera FJ, Yuen DA, Kemp DV (1984) Mass transfer rates along vertical walls in magma chambers and marginal upwelling. Nature 310:764–767

Steck LK, Thurber CH, Fehler MC, Lutter WJ, Roberts PM, Baldridge WS, Stafford DG, Sessions R (1998) Crust and upper mantle P wave velocity structure beneath Valles caldera, New Mexico: results from the Jemez teleseismic tomography experiment. J Geophys Res Solid Earth 103:24,301–24,320

Stephens WE (2001) Polycrystalline amphibole aggregates (clots) in granites as potential I-type restite: an ion microprobe study of rare-earth distributions. Aust J Earth Sci 48:591–601

Takahashi R, Nakagawa M (2012) Formation of a compositionally reverse zoned magma chamber: petrology of the AD 1640 and 1694 eruptions of Hokkaido-Komagatake Volcano, Japan. J Petrol 54: 815–838

Tizzani P, Battaglia M, Zeni G, Atzori S, Berardino P, Lanari R (2009) Uplift and magma intrusion at Long Valley Caldera from InSAR and gravity measurements. Geology 37:63–66

Ubide T, Gale C, Larrea P, Arranz E, Lago M, Tierz P (2014) The Relevance of Crystal Transfer to Magma Mixing: a Case Study in Composite Dykes from the Central Pyrenees. J Petrol 55(8):1535–1559

Uchida E, Endo S, Makino M (2007) Relationship between solidification depth of granitic rocks and formation of hydrothermal ore deposits. Resour Geol 57:47–56

Vegas N, Rodriguez J, Cuevas J, Siebel W, Esteban JJ, Tubía JM, Basei M (2011) The sphene-centered ocellar texture: an effect of grain-supported flow and melt migration in a hyperdense magma mush. J Geol 119:143–157

Vogt JHL (1921) The physical chemistry of the crystallization and magmatic differentiation of igneous rocks. J Geol 28:318–350

Weidendorfer D, Mattsson HB, Ulmer P (2014) Dynamics of magma mixing in partially crystallized magma chambers: textural and petrological constraints from the basal complex of the Austurhorn Intrusion (SE Iceland). J Petrol 55(9):1865–1903

Wilson M (1989) Igneous petrogenesis. Chapman and Hall, London

Wolff JA, Ramos FC (2003) Pb isotope variations among Bandelier Tuff feldspars: no evidence for a long-lived silicic magma chamber. Geology 31:533–536

Wolff JA, Ramos FC, Davidson JP (1999) Sr isotope disequilibrium during differentiation of the Bandelier Tuff, New Mexico: constraints on the crystallization of a large rhyolitic magma chamber. Geology 27:495–498

Wones DR, Eugster HP (1965) Stability of biotite: experiment, theory, and application. Am Mineral 50:1228–1272